Stability of the collinear up-up-down-down magnetic ordering in Ca_3CoMnO_6

Pratap Pal,[1,2,*] Krishnendu Patra,[3,*] Subhajit Nandy,[4] Sudipta Mahana,[5] Jayjit Kumar Dey,[4] Souvik Chatterjee,[6] C. L. Prajapat,[7,8,†] Tapas Paramanik,[9] Dinesh Topwal,[10,11] Amitabh Das,[8,12] Priya Mahadevan,[3] and Debraj Choudhury[1,‡]

[1]*Department of Physics, Indian Institute of Technology Kharagpur, West Bengal 721302, India*
[2]*Department of Materials Science and Engineering, University of Wisconsin, Madison, Wisconsin 53706, USA*
[3]*Department of Condensed Matter and Materials Physics, S. N. Bose National Center for Basic Sciences, Kolkata 700106, India*
[4]*Deutsches Elektronen-Synchrotron DESY, Notkestr. 85, 22607 Hamburg, Germany*
[5]*Rajdhani College, Baramunda Square, Bhubaneswar 751003, India*
[6]*UGC-DAE Consortium for Scientific Research, Kolkata Centre, Sector III, LB-8, Salt Lake, Kolkata 700106, India*
[7]*Technical Physics Division, Bhabha Atomic Research Centre, Mumbai 400085, India*
[8]*Homi Bhabha National Institute, Mumbai 400094, India*
[9]*Department of Physics, National Institute of Technology Andhra Pradesh, Tadepalligudem 534101, India*
[10]*Institute of Physics, Sachivalaya Marg, Bhubaneswar 751005, India*
[11]*Homi Bhabha National Institute, Training School Complex, Anushakti Nagar, Mumbai 400094, India*
[12]*Solid State Physics Division, Bhabha Atomic Research Centre, Mumbai 400085, India*

(Received 6 October 2024; revised 20 September 2025; accepted 1 December 2025; published 22 December 2025)

$Ca_3Co_{2-x}Mn_xO_6$ is a quasi-one-dimensional Ising chain magnet with a unique collinear up-up-down-down ($\uparrow\uparrow\downarrow\downarrow$) magnetic ordering, that gives rise to ferroelectricity below the Néel temperature of 13 K. This unique long-range magnetic ordering, however, was argued to get stabilized only with Co excess (i.e., $x < 1.0$) nonstoichiometric Ca_3CoMnO_6, and not so for the chemically stoichiometric compound $x = 1.0$. Combining several experiments along with first-principles density-functional-based calculations, we elucidate that this unique $\uparrow\uparrow\downarrow\downarrow$ magnetic ordering can be stabilized even in the stoichiometric Ca_3CoMnO_6 (i.e., $x = 1.0$) compound, albeit through the presence of optimum cationic positional disorder, where some Mn and Co ions occupy the trigonal-prismatic (Co sites for the ordered case) and octahedral (Mn-sites for the ordered one) sites respectively through relative tuning of the various magnetic exchange interactions. Specifically, the relative energy stability of the $\uparrow\uparrow\downarrow\downarrow$ magnetic order in Ca_3CoMnO_6 exhibits a nonmonotonic dependency on the extent of cationic disorder with a maximum of around 16% disorder. Thus our study helps to elucidate the mechanism that leads to stabilization of this unique functional $\uparrow\uparrow\downarrow\downarrow$ magnetic ordering in this promising class of multiferroic compounds.

DOI: 10.1103/j9r9-9h3q

I. INTRODUCTION

Type-II multiferroic materials, where ferroelectricity is induced due to magnetic ordering, have been one of the major focus of attention in recent years owing to its strong magnetoelectric effect [1–3]. Depending on the subtle balance among various magnetic interactions, multiferroic systems can host noncollinear as well as collinear magnetic phases [4]. In most cases, the breaking of local inversion symmetry necessary for long-range ferroelectricity, arises from noncollinear magnetic ordering, mediated by strong spin-orbit coupling or inverse Dzyaloshinski-Moriya (DM) interactions [5–7]. In contrast, the collinear magnetism driven ferroelectricity is very rare and has been found to emerge below the magnetic ordering temperature (∼13 K) in an Ising chain magnet $Ca_3Co_{2-x}Mn_xO_6$. Ferroelectricity arises due to the exchange striction effect from the collinear up-up-down-down ($\uparrow\uparrow\downarrow\downarrow$) magnetic ordering (where arrow directions indicate the relative spin orientations of the adjacent transition metal cations) [8–10]. The crystal structure of $Ca_3Co_{2-x}Mn_xO_6$ ($0 \leqslant x \leqslant 1.00$) stabilizes in the *R*-3c (trigonal-family) space group at room temperature as shown in Fig. 1(a). Ca_3CoMnO_6 (i.e., $x = 1.00$) consists of alternating face-shared $Co^{2+}O_6$ trigonal prisms and $Mn^{4+}O_6$ octahedra along the crystallographic *c* axis [11]. Notably, the collinear $\uparrow\uparrow\downarrow\downarrow$ magnetic ordering was found to be stable in $Ca_3Co_{2-x}Mn_xO_6$ for $0.75 < x < 1.0$ (and not for $x = 1.00$) [12], i.e., in compounds with excess Co ions (i.e., $x < 1.0$). $x = 1.05$, i.e., excess Mn ions also partially disturb this long-range ordering. From the crystal field level schemes and corresponding electronic configurations for $Mn^{4+}O_6$ octahedra and $Co^{2+}O_6$ trigonal prisms as shown in Fig. 1(c), we note that the nearest neighbor exchange J_{Co-Mn} is antiferromagnetic (AFM) for ordered structure, and next nearest J'_{Co-Co} or J'_{Mn-Mn} is also AFM. Thus, strong magnetic frustration due to these competing nearest and

[*]These authors contributed equally to this work.
[†]Deceased, contributed to one of the magnetometry measurements.
[‡]Contact author: debraj@phy.iitkgp.ac.in

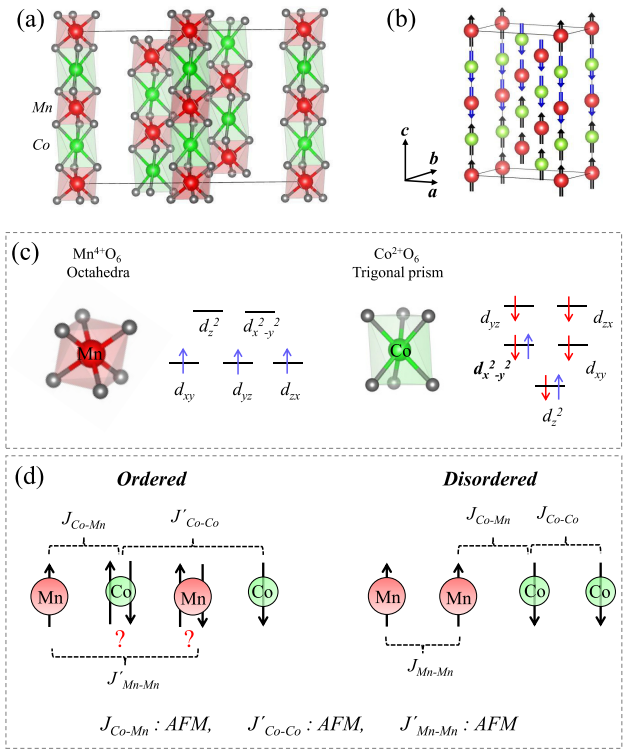

FIG. 1. Schematic illustrations of (a) unit-cell crystal structure of Ca_3CoMnO_6. (b) Up-up-down-down ($\uparrow\uparrow\downarrow\downarrow$) collinear AFM ordering of Mn and Co spins in Ca_3CoMnO_6. (c) Crystal field level schemes and possible electronic configurations for $Mn^{4+}O_6$ octahedra and $Co^{2+}O_6$ trigonal prisms. (d) Schematic illustration of the competing $\uparrow\downarrow\uparrow\downarrow$ and $\uparrow\uparrow\downarrow\downarrow$ orderings responsible for inhomogeneous short-range ordering in the case of cation ordered structure, and the stabilized long-range $\uparrow\uparrow\downarrow\downarrow$ ordering in case of the disordered structure, respectively. Here, the nearest neighbor exchange J_{Co-Mn} is (AFM), while the next nearest J'_{Co-Co} and J'_{Mn-Mn} are also (AFM).

next-nearest intra (or other competing inter chains) interactions, exists in $x \approx 1.00$ and causes destabilization of the exotic $\uparrow\uparrow\downarrow\downarrow$ long-range magnetic ordering [12]. In contrast, the Co-rich ($x = 0.95$) composition helps in reduction of magnetic frustration, which recovers the collinear $\uparrow\uparrow\downarrow\downarrow$ magnetic ordering in $Ca_3Co_{2-x}Mn_xO_6$ compounds [12]. On the other hand, theoretical understandings based on DFT calculations in regards to the relative magnetic ordering stability lack unanimity, as depending on the choice of the exchange correlation functional, either up-down-up-down ($\uparrow\downarrow\uparrow\downarrow$) [9] or up-up-down-down ($\uparrow\uparrow\downarrow\downarrow$, only for very small U values) [13] orderings were found to be stable even for the stoichiometric $x = 1.00$ compound. Experimental efforts toward probing the role of positional disorder on the $\uparrow\uparrow\downarrow\downarrow$ magnetic order stability for the stoichiometric $x = 1.00$ compound are, however, lacking. Thus further experimental and theoretical investigations towards developing a better understanding of the collinear $\uparrow\uparrow\downarrow\downarrow$ magnetic ordering stability in Ca_3CoMnO_6 compound are necessary.

With this goal, we have investigated various $x \approx 1.00$ (i.e., stoichiometric Ca_3CoMnO_6) compounds with different degrees of cationic (i.e., Co or Mn ions) positional disorder. We

TABLE I. Sample nomenclature and synthesis details. All samples were cooled from the annealing temperature of 1473 K to introduce different levels of cationic disorder.

Sample codes	Synthesis conditions	Co-Mn disorder (%)
S_1	very slowly cooled at a rate of 2 K/hour	10 ± 1
S_2	slowly cooled at a rate of 6 K/hour	15 ± 2
S_3	cooled at a rate of 120 K/hour	20 ± 3
S_4	quenched into liquid-N_2	25 ± 5

find that the $\uparrow\downarrow\uparrow\downarrow$ magnetic ordering is competing with the $\uparrow\uparrow\downarrow\downarrow$ magnetic order for an ideal Ca_3CoMnO_6, i.e., without any positional disorder between Co and Mn ions which can give rise to inhomogeneous short-range magnetic ordering, as illustrated in Fig. 1(d). Notably, on the introduction of positional disorder in stoichiometric Ca_3CoMnO_6 ($\sim$10%), some Co ions occupy the octahedral sites while some Mn ions occupy the trigonal prismatic sites. This helps to induce nearest neighbor J_{Mn-Mn} or J_{Co-Co} interactions and leads to stabilization of $\uparrow\uparrow\downarrow\downarrow$ long-range magnetic ordering as shown in Fig. 1(b). Interestingly, the relative stability of $\uparrow\uparrow\downarrow\downarrow$ magnetic ordering for the partial disorder Ca_3CoMnO_6 over that of the ordered one increases with the increase in positional disorder. However, the stability of $\uparrow\uparrow\downarrow\downarrow$ against the $\uparrow\downarrow\uparrow\downarrow$ exhibits a nonmonotonic response, with a maximum around 16% cationic disorder. Thus the $\uparrow\uparrow\downarrow\downarrow$ magnetic ordering seems realizable even in stoichiometric Ca_3CoMnO_6 with the introduction of some cationic positional disorder. Importantly, the presence of very high ($> 16\%$) cationic disorder, however, leads to further destabilization of the $\uparrow\uparrow\downarrow\downarrow$ magnetic long-range order.

II. METHODOLOGY

A. Experimental

Well ground stoichiometric mixture of high purity $CaCO_3$, CoO, and MnO_2, was first pelletized and annealed at 1223 K for 30 hours. Then, the annealed pellet was again ground properly and divided in four different parts. Every part was subsequently subjected to similar heat-treatment at 1473 K for 24 hour [14], followed by different cooling procedures (i.e., different rates of cooling) to introduce varied levels of cationic disorders in polycrystalline Ca_3CoMnO_6. The sample nomenclature details are included in Table I. Chemical stoichiometry was investigated through energy dispersive x-ray (EDX) analyses. Powder x-ray diffraction (XRD) measurements using Cu-K_α and Raman spectroscopic measurements using 514 nm line of Ar^+ laser as an excitation source were carried out at room-temperature. Magnetic measurements were carried out in a SQUID MPMS magnetometer. Temperature dependent neutron powder diffraction was recorded on the PD2 ($\lambda \sim 1.2443$ Å) at Dhruva reactor, Bhabha Atomic Research Centre, Mumbai. The patterns were analysed for crystal and magnetic structure using Fullprof. Spectroscopic XANES (x-ray absorption near edge structure) and EXAFS (extended

x-ray absorption fine structure) data at the Mn and Co K edges were collected at P-64 beamline of Deutsches Elektronen-Synchrotron source, DESY, Hamburg, Germany [15]. XAFS data were measured using Si (111) monochromator with an energy resolution of $\Delta E/E \sim 10^{-4}$. The as-obtained data are processed and analyzed using Athena module. The extended x-ray absorption fine structure (EXAFS) signals were simulated using the Artemis software package. For EXAFS and XANES data analyses, backgrounds of the collected raw data were first subtracted and then normalized using the ATHENA software [16]. Incorporating basic crystallographic information, the EXAFS spectra were fitted with a specific model in the ARTEMIS software [16], in which theoretically calculated spectrum were matched with the experimental spectrum [16–18]. During fitting, k and R ranges were fixed to $3 < k < 13$ Å^{-1} and $1 < R < 3.1$ Å, respectively for Mn K edge, whereas those for Co K-edge were $3 < k < 12$ Å^{-1} and $1 < R < 3.5$ Å, respectively.

B. First-principles calculations

Electronic structure calculations were carried out within a projected augmented wave implementation of density functional theory in the Vienna *ab initio* simulation package (VASP) code [19–22]. The generalized gradient approximation (GGA) [23] to the exchange-correlation function was used. Electron-electron interaction effects were applied to the d-orbitals at both the Mn and Co sites, with a value of U=3 eV for Mn and U=6 eV for Co as in Ref. [9] within the GGA + U implementation by Dudarev [24]. We have considered experimental structural information of the rhombohedral lattice (R-3c) with hexagonal setting [14]. For the convenience of calculation, we extracted the trigonal primitive cell, which consists of only one Co-Mn chain. For the ordered structure, we have taken a cutoff energy of 600 eV for the plane wave expansion and Monkhorst Pack k-point grid of $6 \times 6 \times 6$ for integration over the Brillouin zone [25]. Supercells involving $1 \times 1 \times 2$, $1 \times 1 \times 3$, $1 \times 1 \times 5$ and $2 \times 2 \times 2$ unit cells were used in which the Co and Mn atomic positions were interchanged corresponding to various percentages of disorder. In each case, the atomic positions were optimised for both ↑↓↑↓ and ↑↑↓↓ magnetic configurations with the same values of U. To determine the exchange pathways, we applied maximally localized Wannier functions using the Wannier90-VASP [26,27] interface to map our *ab initio* band structure onto a tight-binding model. We obtained a good tight-binding fit, which enables us to use the complete Hamiltonian and extract both the on-site energies and the hopping interaction strengths. We have then determined the energy gain from each hopping pathway. This involves calculating the band energy, which is nothing but the sum of the occupied eigenvalues within the tight-binding model, with and without the Hamiltonian matrix elements for that hopping pathway.

III. RESULTS AND DISCUSSIONS

A. EXAFS study for the determination of cationic disorder

All the synthesized samples are single phase and found to be crystallized in the R-3c space group, in agreement with earlier reports. Importantly the Co to Mn ratio is similar

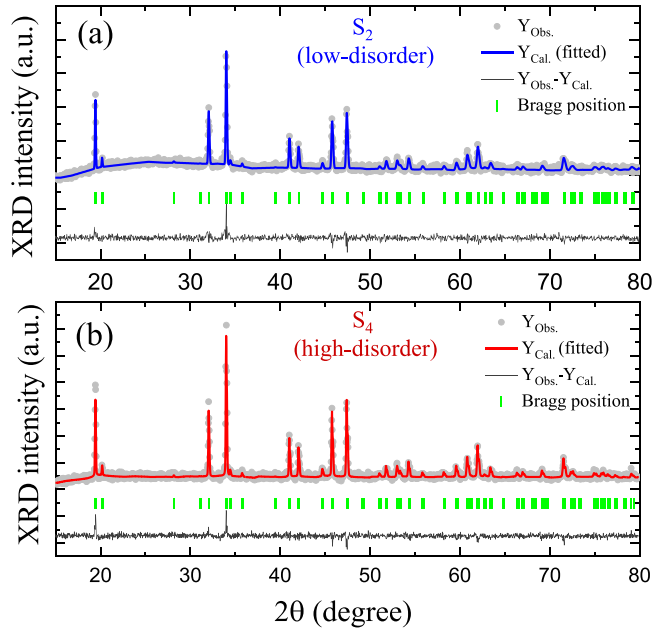

FIG. 2. Rietveld refinements of room-temperature x-ray diffraction spectra for the (a) low-disorder S_2 (with $\chi^2 = 1.34$ and $R_P = 3.59$) and (b) high-disorder S_4 (with $\chi^2 = 1.42$ and $R_P = 3.32$) Ca_3CoMnO_6 compounds.

and close to unity in all the samples, as investigated using energy dispersive x-ray (EDX) analyses, shown in Fig. S1 of Ref. [28]. Systematic cooling at varied rates, after high-temperature annealing process, leads to different levels of cationic positional disorder [29] in the various Ca_3CoMnO_6 (i.e., $x \approx 1.00$) compounds as listed in Table I, which are elucidated using a direct microscopic probe, EXAFS. EXAFS experiments were carried out [30,31] on all the samples at room temperature and at various lower temperatures for two of the extreme compounds from Table I, which exhibit the largest difference in magnetic properties (later to be discussed in the following section), namely S_2 (low-disorder) and S_4 (high-disorder). In this regard, it is also important to note that the presence of high-disorder due to quenching into liquid N_2 (at 77 K) directly from 1473 K does not lead to any significant structural changes in the S_4 compound as compared to low-disordered (S_2) sample as evident from room-temperature XRD refinements and Raman spectroscopic measurements, as shown here in Fig. 2 and Fig. S2 of Ref. [28], respectively. Figures 3(a) and 3(b) display the Fourier transformed EXAFS data of the k^3-weighted spectra (shown in Fig. S4 of Ref. [28]) with the structural-model fittings for Mn and Co K edges of both S_2 (low-disorder) and S_4 (high-disorder) compounds. A good level of fitting of the EXAFS data for all the measured temperatures is achieved for which the corresponding R factors are ∼0.01 and ∼0.006 for Mn and Co K edges, respectively. The Mn (Co) coordination, i.e., number of nearest neighbors, for the absorbing Mn (Co) atom is zero in a perfectly ordered Ca_3CoMnO_6 compound, as Mn and Co ions alternate along the c axis. Presence of cationic positional disorder to some extent could be detected in both the S_2 and S_4 compounds from EXAFS analyses. The percentage of cationic disorder extracted from analyses of

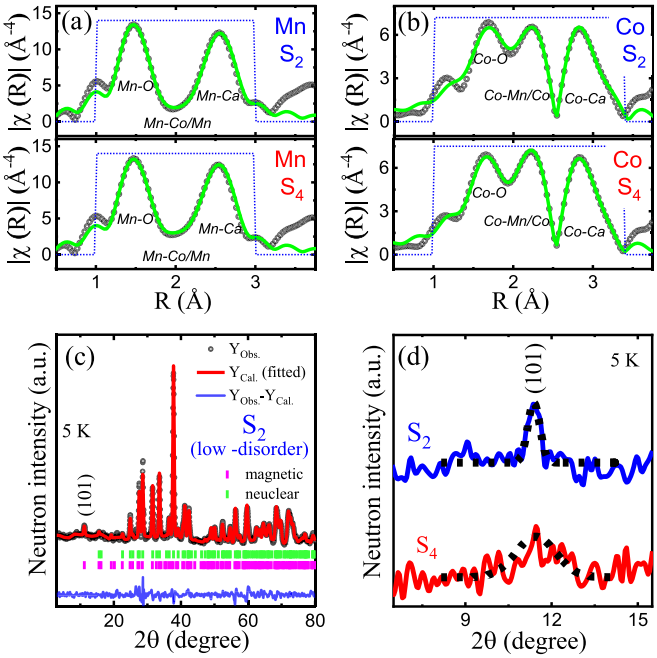

FIG. 3. Fourier transformed spectra of the corresponding k^3-weighted EXAFS data (open circles) along with corresponding fitting (solid lines) for (a) the Mn K edge and (b) the Co K edge respectively at 300 K of the S_2 (low-disorder) and S_4 (high-disorder) compounds. (c) Rietveld refinement of neutron diffraction spectra at 5 K for the S_2 compound. (d) Close-up view of the (101) magnetic peak shows the broadening in case of the high-disorder (S_4) compound, indicating weaker (or short-range) magnetic ordering as compared to that of the sharper peak in case of the low-disorder (S_2) one indicating robust long-range ordering.

both Mn and Co K-edge EXAFS, is higher in the quenched S_4 compound (∼25%) than the slowly-cooled S_2 (∼15%) one, as evident from Table II of Ref. [28]. Mn and Co K-edge XANES spectra [32–36], for all these compounds were also analyzed as shown in Fig. S3 of Ref. [28], where no significant changes in the electronic structure are observed due to cation positional disorder.

B. Neutron diffraction study

Next, to investigate any effect of cationic positional disorder on the ↑↑↓↓ AFM ordering stability of the stoichiometric $x = 1.00$ compound, we employ temperature dependent neutron diffraction measurements focusing on the same two compounds; S_2 (low-disorder) and S_4 (high-disorder), as shown in Fig. S9 of Ref. [28]. We note that there is no structural phase transition down to 1.7 K [37]. Importantly, the magnetic (101) reflection (a signature peak for the unique ↑↑↓↓ AFM ordering [11,12]) becomes prominent below ∼10 K (i.e., at ∼7.5 K) as shown in Fig. S9 of [28]. The Rietveld refinement of the neutron diffraction data has been carried out considering the ↑↑↓↓ [ferromagnetic (FM) nearest neighbor and antiferromagnetic (AFM) next nearest neighbor interactions] Ising chain model between Mn and Co atoms [11], as shown in Fig. 3(c) for the low disorder S_2 compound. Average Mn and Co moments come out to be $1.2 \pm 0.1\ \mu_B$ and $1.0 \pm 0.1\ \mu_B$ for the low disorder S_2 compound (note Table III of Ref. [28]). The obtained cationic disorder from the Rietveld refinement analyses of the neutron diffraction data at 5 K for the S_2 and S_4 samples comes out to be ∼6% higher in S_4 compound than the S_2 compound, which is in qualitative consistency with the cationic disorder estimated from corresponding EXAFS data analyses. Importantly, the (101) magnetic peak is more intense and sharper in case of the low-disorder S_2 compound as compared to a broadened peak of high-disorder S_4, which even becomes clearer from a direct comparison at 5 K, shown in Fig. 3(d). Thus, these observations clearly elucidate that the ↑↑↓↓ magnetic ordering is better stabilized (i.e., higher degree of magnetic correlation) in the low-disorder (∼15%) S_2 compound as compared to the high-disorder (∼25%) S_4 which shows signature of short-range ordering [12]. Although the result of S_2 compound is consistent with previous observation of $x = 0.95$ in $Ca_3Co_{2-x}Mn_xO_6$ [12], the result of weaker long-range ordering even for a higher disordered S_4 compound is surprising, as larger cationic disorder is expected to better stabilize the long-range ordering.

TABLE II. Spin exchange interaction parameters obtained from GGA+U calculations, where a negative sign indicates antiferromagntic exchange interaction.

Magnetic configuration	$J_{Co\text{-}Mn}$ (meV)	$J'_{Mn\text{-}Mn}$ (meV)	$J'_{Co\text{-}Co}$ (meV)
↑↓↑↓	−5	−1	−1

C. Magnetic properties

To further investigate the nature of the dependency of the stabilization of the ↑↑↓↓ AFM ordering on cationic positional disorder, we employ temperature and field dependent dc magnetic measurements. From the variation of magnetization (M) with temperature (T), as shown in Fig. 4(a) and its inset, we note two important features. First, there is a broad transition at ∼13 K (for S_2) in an M-T plot, whereas a second transition is also observed at low temperature of ∼7.5 K [as detected by the peak position in dM/dT plot of Fig. 4(b)]. In this regard, it is important to note that the global long-range AFM ordering indicated by the appearance of (101) magnetic reflection in neutron diffraction measurements also sets in at around 7.5 K (indicating long-range ordering) in Ca_3CoMnO_6 compound, whereas the high-temperature ∼13 K broad magnetic transition is most likely the onset of AFM correlations along the quasi-1D Ising chain. Similar observations were also seen in case of a closely related $MnTiO_3$ where the broad anomaly at ∼100 K in magnetization data indicated the onset of quassi-2D AFM correlations in the a-b plane of $MnTiO_3$ and the low-temperature peak in dM/dT versus T plot at ∼64 K corresponds to the long-range antiferromagnetic ordering in $MnTiO_3$ [38–40]. Interestingly, judging from the sharpness of the AFM transition at T_{3d} in Fig. 4(b), it becomes evident that the global long-range AFM order's stability is more in the low-disorder S_2 compound than the high-disorder S_4 one, which is similar to the observation made from neutron diffraction.

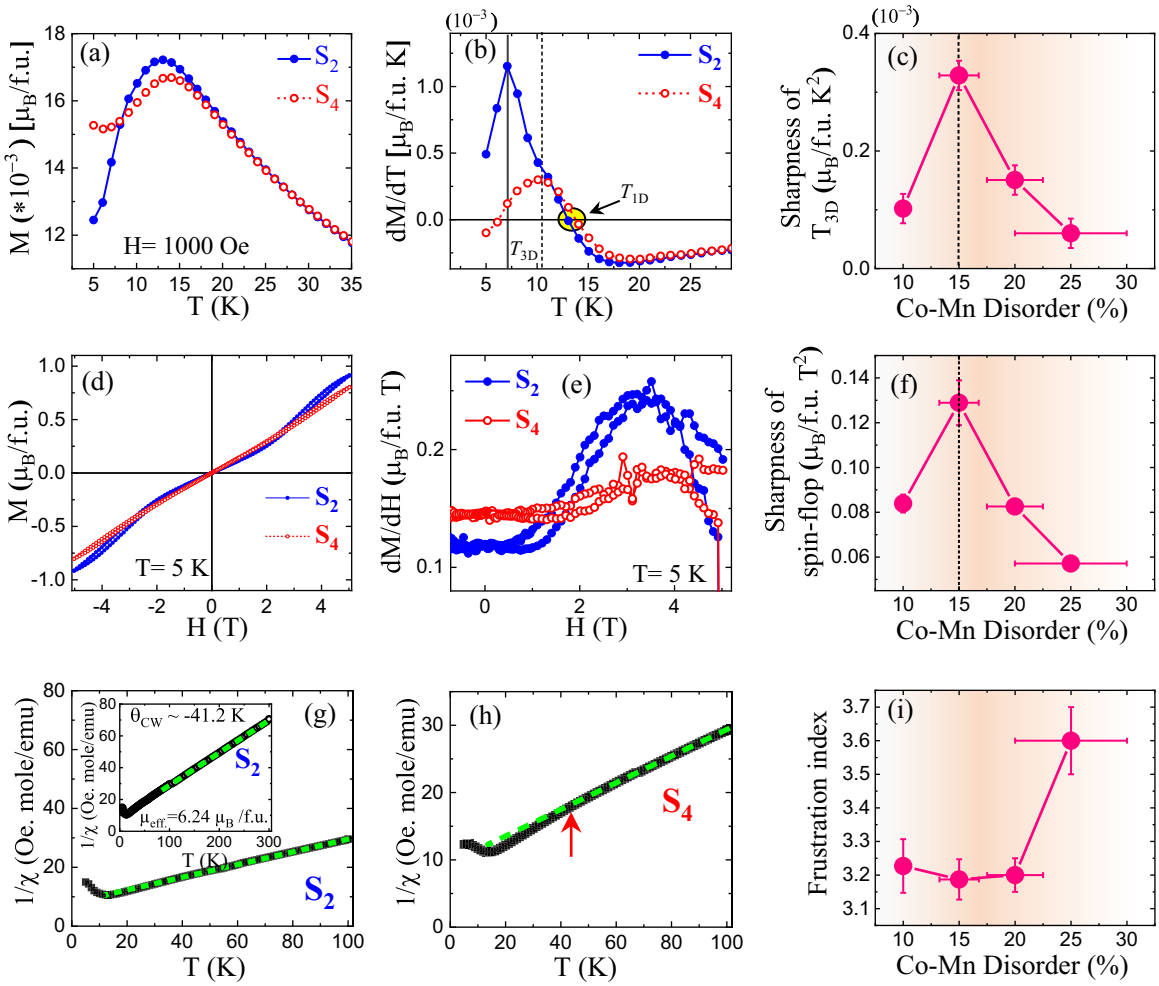

FIG. 4. (a) Temperature (T) dependent magnetization (M) plot (M vs. T) of the low-disorder S_2 and high-disorder S_4 compounds. (b) Corresponding derivative plots. (c) Variation of the "*sharpness*" of magnetic transition, i.e., the maximum change in dM/dT at the 3D long-range $\uparrow\uparrow\downarrow\downarrow$ AFM ordering temperature, divided by the full width at half maximum (FWHM) of the peak for differently disordered compounds. (d) Isothermal magnetization (M) vs applied magnetic field (H) plot at 5 K for the low-disorder S_2 and high-disorder S_4 compounds. (e) Corresponding derivative plots for S_2 and S_4 compounds. (f) Variation of the "*sharpness*" of spin-flop transition, i.e., maximum change in dM/dH plot at the critical magnetic field for metamagnetic phase transition, divided by the FWHM of the peak, with increasing disorder for different compounds. (g) $1/\chi$ vs T plot for the low-disorder S_2 compound shows linear behavior down to the magnetic transition. While its inset shows the corresponding Curie-Weiss fitting. (h) The deviation from linearity at temperatures much higher than the T_N indicating the presence of short-range magnetic ordering in the high-disorder S_4 compound. (i) Variation of the frustration index, as calculated considering the formula $f = |\theta_{CW}|/T_N$ from Curie-Weiss fitting as shown in the inset.

Subsequently from the field dependent magnetization (M-H) measurements in Fig. 4(d), we note that the low-disorder S_2 compound exhibits an almost linear M-H curve at low fields, which however, deviates beyond a critical field and undergoes a metamagnetic like (or spin-flop) transition [41,42]. The spin-flop transition becomes apparent from the appearance of a peak in the derivative of M-H plots, as shown in Fig. 4(e) [43]. It is also important to note that the presence of hysteric M-H loops at high-field beyond the metamagnetic transition indicates its first-order character [41,44]. The sharpness of metamagnetic transition (which is also an effective indicator of the AFM order stability at low field) is more in the low-disorder S_2 compound than the high-disorder S_4 one similar to the observation made in the temperature dependent magnetization data. This result can be understood from the presence of significant short-range magnetic ordering which seems primarily responsible for the broadening of the high-temperature magnetic transition (or otherwise weakening of the long-range ordering) as already seen in the case of the high-disorder S_4 compound in Fig. 4(b). This becomes evident from the deviation of the inverse magnetic susceptibility from a linear monotonic functional dependency contribution at a temperature much higher than the magnetic phase transition in the high-disorder S_4 compound, which, although, is absent in the case of the low-disorder S_2 compound, as shown in Figs. 4(g) and 4(h), respectively.

Now, to understand this unique observation of decreased stability of the $\uparrow\uparrow\downarrow\downarrow$ long-range ordering with increasing disorder, we have considered two more compounds S_1 (with disorder of $\sim$10%, lower than that of the S_2) and S_3 (with disorder of $\sim$20%, higher than that of the S_2, but less than S_4) as listed in Table I. Here the strength of disorder

is $S_4 > S_3 > S_2 > S_1$. From the temperature and field dependent magnetization data shown in Fig. S10 of Ref. [28], we note nonmonotonic response of paramagnetic to AFM phase transition as well as spin-flop transition. To quantify this, we consider the "*sharpness*" parameter defined by the magnitude of the peak in the derivative of magnetization with temperature or field, divided by the full width at half maximum (note Sec. IX of Ref. [28]). Detailed calculation of the sharpness of the magnetic phase transition and the spin-flop transition are described in Figs. S11 and S12 of Ref. [28]. From Figs. 4(c) and 4(f), we note that the "*sharpness*" of both the paramagnetic to AFM and spin-flop transitions exhibits a nonmonotonic dependence with disorder, i.e., initially it increases for small disorder up to S_2 and then again decreases with further increase in cationic disorder, which is intriguing and has not been seen before in this class of Ising-chain magnet.

To understand this observation, we consider magnetic frustration toward the AFM ordering stability. To do so, we did Curie-Weiss fitting of $1/\chi$ versus T data as shown in the inset to Fig. 4(g). It is interesting to note that the magnetic frustration index ($f = |\theta_{CW}|/T_N$) (as described in Ref. [45]), exhibits a similar trend and varies nonmonotonically with the extent of cationic positional disorder as shown in Fig. 4(i). The value of f becomes maximum for the high-disorder S_4 compound with the poorest AFM ordering stability. Thus, it becomes evident that due to the presence of cationic disorder it is the magnetic frustration which primarily controls the $\uparrow\uparrow\downarrow\downarrow$ AFM ordering stability [12,46] in such partially disordered Ca_3CoMnO_6 compounds. In this regard, the effective magnetic moment values, estimated from Curie-Weiss fitting of the high-temperature paramagnetic susceptibility data, as shown in the inset to Fig. 4(f), are $6.46 \pm 0.05\ \mu_B/f.u.$ for the quenched high-disorder S_4 compound and $6.24 \pm 0.02\ \mu_B/f.u.$ for the low-disorder S_2 compound. These results are consistent with the expected spin only magnetic moment for "Mn^{4+}(3/2-Octahedra)-Co^{2+}(3/2-Prismatic)-Mn^{4+}(3/2-Octahedra)-Co^{2+}(3/2-Prismatic)" which is $6\ \mu_B/f.u.$ (here, the number under bracket represents the spin-only moment under the corresponding crystal environment).

D. DFT calculations and understanding of the stability of $\uparrow\uparrow\downarrow\downarrow$ AFM ordering

Subsequently, we attempted to understand the source of stabilization for the up-up-down-down ($\uparrow\uparrow\downarrow\downarrow$) magnetic ground state in the presence of disorder through GGA + U calculation implemented in VASP. First, we have considered four possible collinear magnetic orders; $\uparrow\downarrow\uparrow\downarrow$, $\uparrow\uparrow\downarrow\downarrow$, $\uparrow\downarrow\downarrow\downarrow$, and $\uparrow\uparrow\uparrow\uparrow$ in the Co-Mn-Co-Mn chains for the ordered structure. Atomic positions were optimized within our GGA + U calculation [9] and the total energy of each configuration revealed that $\uparrow\downarrow\uparrow\downarrow$ and $\uparrow\uparrow\downarrow\downarrow$ are the only closest competing ground states, where the former has just 5 meV/f.u. lower energy than the latter (for further details, look at Sec. XIII of Ref. [28]). GGA + U results were mapped onto a Heisenberg model to extract different exchange interaction parameters. The optimized ground state structure was used to calculate the total energy for each of the other magnetic configurations (further details provided in Secs. XIV and XV of Ref. [28]). For the various spin configurations, the total energy (per f.u.) can be expressed as

$$
\begin{aligned}
E_{\uparrow\downarrow\uparrow\downarrow} &= E_0 + 2J_{\text{Co-Mn}} - J'_{\text{Mn-Mn}} - J'_{\text{Co-Co}},\\
E_{\uparrow\uparrow\downarrow\downarrow} &= E_0 + J'_{\text{Mn-Mn}} + J'_{\text{Co-Co}},\\
E_{\uparrow\downarrow\downarrow\downarrow} &= E_0 + J'_{\text{Mn-Mn}} - J'_{\text{Co-Co}},\\
E_{\uparrow\uparrow\uparrow\uparrow} &= E_0 - 2J_{\text{Co-Mn}} - J'_{\text{Mn-Mn}} - J'_{\text{Co-Co}}.
\end{aligned}
$$

Here values of magnetic moments are absorbed in the exchange interaction parameters. J is the spin-exchange parameter and E_0 is the spin independent constant of total energy. From these equations, we obtained the exchange parameters listed in Table II. Interestingly, all these Js are anti-ferromagnetic and $J_{\text{Co-Mn}}$ plays the dominant role in making the $\uparrow\downarrow\uparrow\downarrow$ configuration compete with the $\uparrow\uparrow\downarrow\downarrow$ one. For the $\uparrow\uparrow\downarrow\downarrow$ configuration there is no contribution from Co-Mn exchange interactions. Thus, due to such a strong competition between $\uparrow\uparrow\downarrow\downarrow$ and $\uparrow\downarrow\uparrow\downarrow$, the long-range order is disturbed and significant short-range order is evolved in perfectly ordered Ca_3CoMnO_6. Alternately, exchange striction in the $\uparrow\uparrow\downarrow\downarrow$ configuration can lead to a nonvanishing contribution to the energy from nearest neighbor Mn-Co interactions, though this is very small. Short-range incommensurate magnetic order has been reported for stoichiometric Ca_3CoMnO_6 [12]. Our Monte-Carlo calculations also suggest presence of multiple degenerate magnetic states for the cation-ordered Ca_3CoMnO_6 (methodology and results included in Sec. XVI of Ref. [28]).

As the GGA + U method in DFT calculations often correctly reproduces the relative energies between magnetic states and electronic structures, we have introduced antisite disorder in Ca_3CoMnO_6 considering different supercells and interchanging the positions of Co and Mn atoms depending on the percentages of disorder as shown by a representative example in Figs. 5(a) and 5(b). Since $\uparrow\uparrow\downarrow\downarrow$ and $\uparrow\downarrow\uparrow\downarrow$ magnetic orderings are the two closely competing states in the ordered system, the relative energy differences between $\uparrow\uparrow\downarrow\downarrow$ and $\uparrow\downarrow\uparrow\downarrow$ serve as the basis for examining the stability of the $\uparrow\uparrow\downarrow\downarrow$ configuration in case of disorder in the system. We have performed *ab initio* calculations for 6.25%, 10%, 16.67%, and 25% disorder imposing $\uparrow\uparrow\downarrow\downarrow$ and $\uparrow\downarrow\uparrow\downarrow$ magnetic configurations. The energy differences between these structures, as plotted in Fig. 5(c) (also tabulated in Sec. XV of Ref. [28]), strongly indicate the nonmonotonic dependence of the $\uparrow\uparrow\downarrow\downarrow$ magnetic ordering stability with cationic disorder. Thus obtained theoretical results are in broad consistence with the experimental results. For the ideal cation-ordered Ca_3CoMnO_6, theoretically, the $\uparrow\downarrow\uparrow\downarrow$ configuration is strongly competing with the $\uparrow\uparrow\downarrow\downarrow$ configuration. However, with progressive incorporation of cation positional disorder for our calculations, the relative stability of the $\uparrow\uparrow\downarrow\downarrow$ configuration continues to increase and becomes the ground state magnetic configuration for ~16% cation disorder, as seen in Fig. 5(c). With further increase in cationic disorder beyond ~16%, the competition between these two energetically close magnetic configurations seems to be the primary source of significant short-range ordering observed for our higher disordered compound (S_4). Whereas Co^{2+}-O and Mn^{4+}-O bond lengths are similar to the ordered results, some Mn^{3+}-O

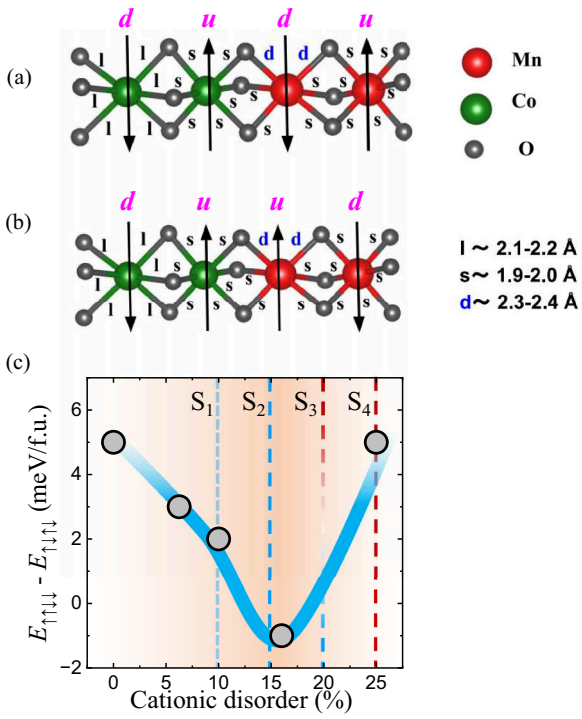

FIG. 5. Co-Mn chains for the optimized structure with 16.67% disorder for (a) ↓↑↓↑ magnetic ordering and (b) ↓↑↑↓ magnetic ordering. (c) Variation of $E_{\uparrow\uparrow\downarrow\downarrow}$-$E_{\uparrow\downarrow\uparrow\downarrow}$ with cationic positional disorder highlighting the stability of ↑↑↓↓ ordering.

bonds are found to be distorted and larger (2.33 to 2.4 Å) as shown in Figs. 5(a) and 5(b), which reduces hopping via the pathway Co-O-Mn. However, in some regions, Co and Mn atoms as nearest neighbors can lead to an effective gain for the ↑↑↓↓ configuration.

We know from an analysis of the hopping pathways that the exchange mechanism happens through the oxygen. So, for the disordered system, some Mn-O bonds are distorted and higher than other average Mn-O bonds so the effective gain from hopping in this path is reduced, as shown in Fig. 5 (similar observation was also seen from the deduction of respective bond distances via structural refinements of EXAFS data as shown in Fig. S8 of Ref. [28]). So qualitatively we can say that nearest neighbor exchange interactions in both ↑↑↓↓ and ↑↓↑↓ configurations are reduced in the disordered region. Interestingly, there is no nearest neighbor exchange term ($J_{Co\text{-}Mn}$) in the spin exchange expressions for ↑↑↓↓ ordered system. However, for the disordered system in some regions, Co-Co and Co-Mn (Mn-Mn and Co-Mn) are nearest neighbors. So, there is a contribution from the nearest neighbor exchange. Therefore, with disorder ↑↑↓↓ can gain stability and become the ground state. In a nutshell, the main route toward ↑↑↓↓ long-range ordering is to reduce the contribution from the nearest neighbor exchange interaction.

IV. SUMMARY

In summary, by combining various experimental results along with first-principles DFT-based calculations, we elucidate that the unique ↑↑↓↓ collinear magnetic ordering that gives rise to ferroelectricity, can be engineered in stoichiometric Ca_3CoMnO_6 through the presence of an optimal amount of cationic positional disorder. The increased stabilization of the ↑↑↓↓ magnetic ordering over the competing ↑↓↑↓ ordering becomes feasible through the introduction of nearest neighbor Co-Co and Mn-Mn exchange interactions in the positional disordered compound, which is qualitatively similar with previous observations. However, the presence of a relatively large cationic disorder introduces significant magnetic frustration and destabilizes the ↑↑↓↓ magnetic ordering in Ca_3CoMnO_6. Thus our study broadens the scope of the investigation by capturing the nonmonotonic dependence of ↑↑↓↓ magnetic ordering on extent of cationic disorder (also illustrated in Fig. S13 of Ref. [28]), which we believe is a key insight in this interesting class of materials associated with magnetoelectric-multiferroic properties.

ACKNOWLEDGMENTS

P.P. would like to acknowledge the financial support from Ministry of Human Resource Development (MHRD), Government of India from June 2015 to June 2021 during the Ph.D. program. D.C. acknowledges STARS, MHRD, India (funding under Project File No. STARS/APR2019/NS/238/FS) and BRNS, Department of Atomic Energy (DAE), India (funding through Sanction No. 37(3)/20/23/2016-BRNS), for financial support. We acknowledge DESY (Hamburg, Germany), a member of the Helmholtz Association HGF, for the provision of experimental facilities. Parts of this research were carried out at PETRA III, P64, and we would like to thank Aleksandr Kalinko for beamline guidance. P.M. thanks Science and Engineering Research Board for support through the project SERB-POWER (SPF/2021/000066). K.P. acknowledges Param Rudra computing facility under the National Supercomputing Mission at SNBNCBS, Kolkata by Government of India.

[1] N. A. Spaldin and R. Ramesh, Advances in magnetoelectric multiferroics, Nat. Mater. **18**, 203 (2019).
[2] T. Kimura, T. Goto, H. Shintani, K. Ishizaka, T. Arima, and Y. Tokura, Magnetic control of ferroelectric polarization, Nature (London) **426**, 55 (2003).
[3] Y. H. Chu, L. W. Martin, M. B. Holcomb, M. Gajek, S. J. Han, Q. He, N. Balke, C. H. Yang, D. Lee, W. Hu, Q. Zhan, P. L. Wang, A. F. Rodriguez, A. Scholl, S. X. Wang, and R. Ramesh, Electric-field control of local ferromagnetism using a magnetoelectric multiferroic, Nat. Mater. **7**, 478 (2008).
[4] M. V. Gvozdikova, T. Ziman, and M. E. Zhitomirsky, Helicity, anisotropies, and their competition in a multiferroic magnet: Insight from the phase diagram, Phys. Rev. B **94**, 020406(R) (2016).
[5] D. Khomskii, Classifying multiferroics: Mechanisms and effects, Physics **2**, 20 (2009).

[6] M. Fiebig, T. Lottermoser, D. Meier, and M. Trassin, The evolution of multiferroics, Nat. Rev. Mater. **1**, 16046 (2016).

[7] C. Lu and J. M. Liu, $DyMnO_3$: A model system of type-II multiferroics, J. Materiomics **2**, 213 (2016).

[8] Y. J. Choi, H. T. Yi, S. Lee, Q. Huang, V. Kiryukhin, and S. W. Cheong, Ferroelectricity in an Ising chain magnet, Phys. Rev. Lett. **100**, 047601 (2008).

[9] H. Wu, T. Burnus, Z. Hu, C. Martin, A. Maignan, J. C. Cezar, A. Tanaka, N. B. Brookes, D. I. Khomskii, and L. H. Tjeng, Ising magnetism and ferroelectricity in Ca_3CoMnO_6, Phys. Rev. Lett. **102**, 026404 (2009).

[10] P. Ding, L. Li, Y. J. Guo, Q. Y. He, X. S. Gao, J. M. Liu, and S. W. Cheong, Influence of Co:Mn ratio on multiferroicity of around $x\sim1.0$, Appl. Phys. Lett. **97**, 032901 (2010).

[11] S. D. Kaushik, S. Rayaprol, J. Saha, N. Mohapatra, V. Siruguri, P. D. Babu, S. Patnaik, and E. V. Sampathkumaran, Magnetoelectric coupling in Ca_3CoMnO_6, J. Appl. Phys. **108**, 084106 (2010).

[12] V. Kiryukhin, S. Lee, W. Ratcliff, Q. Huang, H. T. Yi, Y. J. Choi, and S. W. Cheong, Order by static disorder in the Ising chain magnet $Ca_3Co_{2-x}Mn_xO_6$, Phys. Rev. Lett. **102**, 187202 (2009).

[13] Y. Zhang, H. J. Xiang, and M. H. Whangbo, Interplay between Jahn-Teller instability, uniaxial magnetism, and ferroelectricity in Ca_3CoMnO_6, Phys. Rev. B **79**, 054432 (2009).

[14] V. G. Zubkov, G. V. Bazuev, A. P. Tyutyunnik, and I. F. Berger, Synthesis, crystal structure, and magnetic properties of quasi-one-dimensional oxides Ca_3CuMnO_6 and $Ca_3Co_{1+x}Mn_{1-x}O_6$, J. Solid State Chem. **160**, 293 (2001).

[15] W. A. Caliebe, V. Murzin, A. Kalinko, and M. Görlitz, High-flux XAFS-beamline P64 at PETRA III, AIP Conf. Proc. **2054**, 060031 (2019).

[16] B. Ravel, and M. Newville, *ATHENA, ARTEMIS, HEPHAESTUS*: data analysis for X-ray absorption spectroscopy using *IFEFFIT*, J. Synchrotron Radiat. **12**, 537 (2005).

[17] J. J. Rehr, and R. C. Albers, Theoretical approaches to x-ray absorption fine structure, Rev. Mod. Phys. **72**, 621 (2000).

[18] J. J. Rehr, J. J. Kas, M. P. Prange, A. P. Sorini, Y. Takimoto, and F. Vial, *Ab initio* theory and calculations of X-ray spectra, C. R. Phys. **10**, 548 (2009).

[19] P. E. Blöchl, Projector augmented-wave method, Phys. Rev. B **50**, 17953 (1994).

[20] G. Kresse and J. Hafner, *Ab initio* molecular dynamics for liquid metals, Phys. Rev. B **47**, 558 (1993).

[21] G. Kresse and J. Hafner, *Ab initio* molecular-dynamics simulation of the liquid-metal–amorphous-semiconductor transition in germanium, Phys. Rev. B **49**, 14251 (1994).

[22] G. Kresse and J. Furthmüller, Efficient iterative schemes for *ab initio* total-energy calculations using a plane-wave basis set, Phys. Rev. B **54**, 11169 (1996).

[23] J . P. Perdew, K. Burke, and M. Ernzerhof, Generalized gradient approximation made simple, Phys. Rev. Lett. **77**, 3865 (1996).

[24] S. L. Dudarev, G. A. Botton, S. Y. Savrasov, C. J. Humphreys, and A. P. Sutton, Electron-energy-loss spectra and the structural stability of nickel oxide: An LSDA+U study, Phys. Rev. B **57**, 1505 (1998).

[25] H. J. Monkhorst and J. D. Pack, Special points for Brillouin-zone integrations, Phys. Rev. B **13**, 5188 (1976).

[26] A. A. Mostofi, J. R. Yates, Y.-S. Lee, I. Souza, D. Vanderbilt, and N. Marzari, An updated version of wannier90: A tool for obtaining maximally-localised Wannier functions, Comput. Phys. Commun. **185**, 2309 (2014).

[27] C. Franchini, R. Kováčik, M. Marsman, S. S. Murthy, J. He, C. Ederer, and G. Kresse, Maximally localized Wannier functions in $LaMnO_3$ within $PBE + U$, hybrid functionals and partially self-consistent GW: an efficient route to construct *ab initio* tight-binding parameters for e_g perovskites, J. Phys.: Condens. Matter **24**, 235602 (2012).

[28] See Supplemental Material at http://link.aps.org/supplemental/10.1103/j9r9-9h3q for extended EDAX, Raman, EXAFS, neutron and first-principle calculation data.

[29] M. Morin, E. Cańevet, A. Raynaud, M. Bartkowiak, D. Sheptyakov, V. Ban, M. Kenzelmann, E. Pomjakushina, K. Conder, and M. Medarde, Tuning magnetic spirals beyond room temperature with chemical disorder, Nat. Commun. **7**, 13758 (2016).

[30] V. R. Mastelaro, and E. D. Zanotto, X-ray absorption fine structure (XAFS) studies of oxide glasses—A 45-Year overview, Materials **11**, 204 (2018).

[31] P. A. O'Day, J. J. Rehr, S. I. Zabinsky, and G. E. Brown, Jr., Extended X-ray absorption fine structure (EXAFS) analysis of disorder and multiple-scattering in complex crystalline solids, J. Am. Chem. Soc. **116**, 2938 (1994).

[32] A. Manceau, M. A. Marcus, and S. Grangeon, Determination of Mn valence states in mixed-valent manganates by XANES spectroscopy, Am. Mineral. **97**, 816 (2012).

[33] T. Ye, S. Li, X. Wu, M. Xu, X. Wei, K. Wang, H. Bao, J. Wang, and J Chen, Sol–gel preparation of efficient red phosphor $Mg_2TiO_4 : Mn^{4+}$ and XAFS investigation on the substitution of Mn^{4+} for Ti^{4+}, J. Mater. Chem. C **1**, 4327 (2013).

[34] L. Chen, T. Mashimo, C. Iwamoto, H. Okudera, E. Omurzak, H. S. Ganapathy, H. Ihara, J. Zhang, Z. Abdullaeva, S. Takebe, and A. Yoshiasa, Synthesis of novel CoC_x@C nanoparticles, Nanotechnology **24**, 045602 (2013).

[35] M. P. F. García, P. Gorria, M. Sevilla, A. B. Fuertes, R. Boada, J. Chaboy, G. Aquilanti, and J. A. Blanco, Co nanoparticles inserted into a porous carbon amorphous matrix: the role of cooling field and temperature on the exchange bias effect, Phys. Chem. Chem. Phys. **13**, 927 (2011).

[36] J. A. Sigrist, M. W. Gaultois, and A. P. Grosvenor, Investigation of the Fe K-edge XANES Spectra from $Fe_1 - xGa_xSbO_4$: Local versus nonlocal excitations, J. Phys. Chem. A **115**, 1908 (2011).

[37] J. Shi, J. D. Song, J. C. Wu, X. Rao, H. L. Che, Z. Y. Zhao, H. D. Zhou, J. Ma, R. R. Zhang, L. Zhang, X. G. Liu, X. Zhao, and X. F. Sun, Ferroelectricity of structural origin in the spin-chain compounds $Ca_3Co_{2-x}Mn_xO_6$, Phys. Rev. B **96**, 064112 (2017).

[38] N. Mufti, G. R. Blake, M. Mostovoy, S. Riyadi, A. A. Nugroho, and T. T. M. Palstra, Magnetoelectric coupling in $MnTiO_3$, Phys. Rev. B **83**, 104416 (2011).

[39] R. K. Maurya, N. Singh, S. K. Pandey, and R. Bindu, Evidence of spin lattice coupling in $MnTiO_3$: An x-ray diffraction study, EPL **110**, 27007 (2015).

[40] P. Pal, A. Rahaman, J. Brar, R. Bindu, and D. Choudhury, Competing magnetic interactions driven tuning of spin-flop field and anomalous thermal expansion in $MnTi_{1-x}Mn_xO_3$, J. Appl. Phys. **132**, 183905 (2022).

[41] Z. W. Ouyang, N. M. Xia, Y. Y. Wu, S. S. Sheng, J. Chen, Z. C. Xia, L. Li, and G. H. Rao, Short-range ferromagnetic correlations in the spin-chain compound Ca_3CoMnO_6, Phys. Rev. B **84**, 054435 (2011).

[42] J. W. Kim, Y. Kamiya, E. D. Mun, M. Jaime, N. Harrison, J. D. Thompson, V. Kiryukhin, H. T. Yi, Y. S. Oh, S. W. Cheong, C. D. Batista, and V. S. Zapf, Multiferroicity with coexisting isotropic and anisotropic spins in $Ca_3Co_{2-x}Mn_xO_6$, Phys. Rev. B **89**, 060404(R) (2014).

[43] F. L. A. Machado, P. R. T. Ribeiro, J. Holanda, R. L. Rodríguez-Suárez, A. Azevedo, and S. M. Rezende, Spin-flop transition in the easy-plane antiferromagnet nickel oxide, Phys. Rev. B **95**, 104418 (2017).

[44] S. Rayaprol, K. Sengupta, and E. V. Sampathkumaran, Magnetic behavior of quasi-one-dimensional oxides $Ca_3Co_{1+x}Mn_{1-x}O_6$, Solid State Commun. **128**, 79 (2003).

[45] A. P. Ramirez, Geometrically frustrated matter-magnets to molecules, Annu. Rev. Mater. Sci. **24**, 453 (1994).

[46] S. Niitaka, K. Yoshimura, K. Kosuge, M. Nishi, and K. Kakurai, Partially disordered antiferromagnetic phase in Ca_3CoRhO_6, Phys. Rev. Lett. **87**, 177202 (2001).